Hierarchical Growth of Mixed Ammonium Molybdenum/Tungsten Bronze Nanorods

Alexej Michailovski, Frank Krumeich, and Greta R. Patzke*

Laboratory of Inorganic Chemistry, ETH Hönggerberg, Wolfgang-Pauli-Str. 10, CH-8093 Zürich, Switzerland

Received November 24, 2003. Revised Manuscript Received February 3, 2004

Mixed ammonium molybdenum/tungsten bronzes are available in nanoscopic form via a straightforward solvothermal synthesis in acidic media. The emerging rods exhibit average lengths below 1 μm and diameters of 20−30 nm. They self-organize into manifold microscale patterns. The growth of mixed nanorods proceeds within a wide solvothermal parameter window (time, temperature, and pH). Intermediate morphologies give indications of a possible growth mechanism. The complex nanorod arrangements exhibit BET surface areas around 89 m^2g^{-1}, and they withstand heating to 450 °C.

Introduction

During the past decade, considerable progress in the synthesis of nanoparticles has been achieved.[1−5] Great emphasis has been placed upon the development of anisotropic nanoparticles, because they can be aligned and functionalized for future nanotechnological purposes.[6] Solvothermal syntheses deliver such nanomaterials via straightforward and scalable one-step routines.[7−9] The industrial manufacturing of nanoparticles requires predictive design rules, and these can be derived only by understanding the fundamentals of solvothermal processes. Hand in hand with nanochemistry, the "chemistry of form" has been established as an important branch of materials chemistry.[10,11]

Nanoscale transition metal oxides are of special interest because of their multitude of important properties.[12] Molybdenum- and tungsten-based oxides in particular offer a rich structural chemistry so that they are in the focus of *chimie douce* approaches.[13] Their vast application potential can be outlined here only briefly.

MoO_3 and WO_3 both provide strong surface acid sites in the +5/+6 oxidation states together with metal-oxide double bonds. Their catalytic activity is exploited for manifold industrially important reactions, such as hydrocarbon conversions[14] and numerous redox or acid−base reactions.[15] These catalysts can be further enhanced through the formation of mixed oxides with V_2O_5 or Nb_2O_5. Despite their efficiency, such mixed oxide materials remain to be explored: MoVW oxides, for example, belong to the most selective and active oxide catalyst systems, and they find use in the oxidation of acrolein to acrylic acid.[16] The individual functions of the three transition metal cations, however, are not fully understood up to now. Recently, $(Mo_xW_{1-x})O_3$ ($x < 0.5$) solid solutions were found to be highly active and selective in methanol oxidation.[17] The functionalization of MCM-48 mesoporous silica with tungsten and molybdenum metal centers has been studied as well with respect to catalytic peroxide activation.[18]

Furthermore, molybdenum and tungsten oxide represent important sensor materials: MoO_3 exhibits sensitivity toward NH_3, H_2, CO, and NO_2,[19] and WO_3 responds well to NO_x and O_3.[20] These sensor properties can again be improved through the preparation of mixed oxides: $W_{0.9}Mo_{0.1}O_3$, for example, shows strong sensitivity to gases in low concentrations in air (O_3 or NO_x), independent of changes in the relative humidity.[21] Highly selective (W, Mo)O_x sensors could play an important role in the environmental detection of NO_2,[20] and their response toward O_2 is increased with respect to the binary sensors as well.[22] Finally, mixed molyb-

* To whom correspondence should be addressed. Tel.: +41-1-632 67 43. Fax: +41-1-632 11 49. E-mail: patzke@inorg.chem.ethz.ch.

(1) Rao, C. N. R.; Cheetham, A. K. *J. Mater. Chem.* **2001**, *11*, 2887.
(2) Rao, C. N. R.; Kulkarni, G. U.; Thomas, P. J.; Edwards, P. P. *Chem. Eur. J.* **2002**, *8*, 29.
(3) Kwan, S.; Kim, F.; Akana, J.; Yang, P. *Chem. Commun.* **2001**, 447.
(4) Pan, Z. W.; Dai, Z. R.; Wang, Z. L. *Science* **2001**, *291*, 1947.
(5) Tenne, R. *Prog. Inorg. Chem.* **2001**, *50*, 269.
(6) Patzke, G. R.; Krumeich, F.; Nesper, R. *Angew. Chem., Int. Ed.* **2002**, *41*, 2446.
(7) Niederberger, M.; Krumeich, F.; Muhr, H.-J.; Müller, M.; Nesper, R. *J. Mater. Chem.* **2001**, *11*, 1941.
(8) Patzke, G. R.; Michailovski, A.; Krumeich, F.; Nesper, R.; Grunwaldt, J.-D.; Baiker, A. *Chem Mater.* **2004**, *6*, 1126.
(9) Lou, X. W.; Zeng, H. C. *Chem. Mater.* **2002**, *14*, 4781.
(10) Mann, S. *Angew. Chem., Int. Ed.* **2000**, *39*, 3392.
(11) Ozin, G. A.; Yang H.; Coombs, N. *Nature* **1997**, *386*, 692.
(12) Rao, C. N. R.; Raveau, B. *Transition Metal Oxides*; VCH Publishers: New York, 1995.
(13) Figlarz, M. *Prog. Solid St. Chem.* **1989**, *19*, 1.
(14) Moreno-Castilla, C.; Pérez-Cadenas, A. F.; Maldonado-Hódar, F. J.; Carrasco-Marín, F.; Fierro, J. L. G. *Carbon* **2003**, *41*, 1157.
(15) Haber, J.; Lalik, E. *Catal. Today* **1997**, *33*, 119.
(16) Ovitsver, O.; Uchida, Y.; Mestl, G.; Weinberg, G.; Blume, A.; Jäger, J.; Dieterle, M.; Hibst, H.; Schlögl, R. *J. Mol. Catal. A* **2002**, *185*, 291.
(17) Ivanov, K.; Mitov, I.; Krustev, S. *J. Alloys Compd.* **2000**, *309*, 57.
(18) Morey, M. S.; Bryan, J. D.; Schwarz, S.; Stucky, G. D. *Chem. Mater.* **2000**, *12*, 3435.
(19) Prasad, A. K.; Gouma, P. I. *J. Mater. Sci.* **2003**, *38*, 4347.
(20) Galatsis, K.; Li, Y.; Wlodarski W.; Cantalini, C.; Passacantando, M.; Santucci, S. *J. Sol-Gel Sci. Technol.* **2003**, *26*, 1097.
(21) Merdrignac-Conanec, O.; Moseley, P. T. *J. Mater. Chem.* **2002**, *12*, 1779.
(22) Galatsis, K.; Li, Y. X.; Wlodarski, W.; Kalantar-zadeh, K. *Sens. Actuators B* **2001**, *77*, 478.

10.1021/cm0311731 CCC: $27.50
Published on Web 03/19/2004

denum tungsten oxides have been discussed as hydrogen storage materials.[23]

To exploit their outstanding properties for future nanotechnology, nanorods of MoO_3 have been prepared via manifold approaches[24] including thermal evaporation/oxidation techniques,[25] electrochemical deposition,[26] and solvothermal methods.[7−9,27] The preparative spectrum for the fabrication of WO_3 nanorods is equally wide, ranging from sonochemical syntheses[28] over physical deposition processes[29] and colloidal precipitations[30] to template-directed methods.[31] Considerably less is known about the synthesis of mixed molybdenum/tungsten oxide nanoparticles.

Whereas the hexagonal $(NH_4)_xWO_3$ bronzes have been extensively characterized,[32−35] $(NH_4)_x(W,Mo)O_3$ bronzes have not been described in comparable detail. So this study is dedicated to the solvothermal synthesis of nanoscopic $(NH_4)_x(W,Mo)O_3$ bronzes as a contribution to the nanoscale morphology design of mixed oxides. The experimental strategy was devised against the following background. (1) The structure of mixed $W_{1-x}Mo_xO_3$ systems depends on the preparative pathway: conventional thermochemical methods point to the existence of several crystallographic phases. Most of them are related to the ReO_3-based orthorhombic and monoclinic forms of WO_3.[36] *Chimie douce* routes starting from the mixed $(W,Mo)O_3 \cdot 0.33H_2O$ acid series give access to $(W,Mo)O_3$ solid solutions as well. Their tungsten-rich members ($0.1 < x < 0.5$) adopt a metastable hexagonal structure.[13] Novel orthorhombic $W_{1-x}Mo_xO_3$ oxides can furthermore be generated via the deintercalation of layered amine adducts.[37] (2) Both molybdenum and tungsten oxide can be obtained in nanostructured form by solvothermal procedures: MoO_3 fibers[7−9] are generated from yellow molybdic acid ($MoO_3 \cdot 2H_2O$),[7,8] and several tungsten oxides[38,39] are accessible via ammonium metatungstate, $(NH_4)_6H_2W_{12}O_{41} \cdot H_2O$.

Therefore, the combined solvothermal reaction of yellow molybdic acid and ammonium metatungstate was investigated with respect to the formation of mixed nanoscopic molybdenum/tungsten oxides.

Experimental Section

In a typical experiment, 297 mg of $(NH_4)_6H_2W_{12}O_{41} \cdot H_2O$ (Riedel-deHaën) and 144 mg of $MoO_3 \cdot 2H_2O$ (synthesized according to the literature[40]) were added together with 1.5 mL of diluted glacial acetic acid (25 vol %) to a Teflon-lined stainless steel autoclave with the capacity of 23 mL. The autoclave was then sealed, heated at 180 °C for 4 days, and subsequently cooled to room temperature. The precipitate was collected after filtration, washed with distilled water, ethanol, and ether, and dried in air. X-ray powder analysis was conducted on a STOE STADI-P2 diffractometer in transmission mode (flat sample holders, germanium monochromated Cu Kα radiation) equipped with a position sensitive detector (resolution ~0.01° in 2θ). For transmission electron microscopy (TEM), the material was deposited on a perforated carbon foil supported on a copper grid. The scanning transmission electron microscopy (STEM) image was recorded with a HAADF detector on a Philips Tecnai 30F microscope, operated at 300 kV (field emission cathode). In the STEM mode, the electron beam was placed on a selected spot, and an elemental analysis by energy-dispersive X-ray spectroscopy (EDS, EDAX detector) was performed there. All samples were analyzed by EDS in a Philips CM 30 ST equipped with a Noran Voyager System, and approximate values for the W/Mo ratio were obtained (Table 1). For scanning electron microscopy (SEM), performed on a LEO 1530 (FEG) microscope with 1 keV electrons, samples were dispersed in ethanol and subsequently deposited on a silicon wafer. FTIR spectra were recorded on a Perkin-Elmer Spectrum 2000 FTIR spectrometer in the range from 500 to 4000 cm^{-1}. C, H, and N analysis was carried out by means of combustion test methods on a LECO CHN-900. Nitrogen absorption was measured at 77 K with a TriStar 3000 apparatus. Prior to the measurement, the sample was degassed at 80 °C for several hours under vacuum. The surface area was determined by the BET method. DTA/TG measurements were performed on a NETZSCH STA 409 C apparatus between 20 and 1500 °C with a heating rate of 10 K min^{-1} in argon atmosphere.

Results

Formation of Mixed Nanorods from $MoO_3 \cdot 2H_2O$ and Ammonium Metatungstate. Yellow molybdic acid, $MoO_3 \cdot 2H_2O$, exhibits a characteristic monoclinic layer structure with interlayer water molecules.[41] The template-free solvothermal treatment of $MoO_3 \cdot 2H_2O$ under acidic conditions leads to the quantitative formation of MoO_3 nanorods with microscale lengths and diameters of 100−150 nm.[8] Ammonium metatungstate provides considerably smaller nanorods of $(NH_4)_{0.26}WO_3$ with diameters in the 30−50 nm range and lengths between 100 and 700 nm when subjected to analogous reaction conditions.[38] The Keggin structure of the starting material is transferred into a nanoscopic hexagonal tungsten bronze. As a consequence, the formation of mixed nanoscale oxides from $MoO_3 \cdot 2H_2O$ and ammonium metatungstate was investigated in terms of combined solvothermal reactions, and the resulting trends are listed in Table 1 and Figures 1 and 2. The products can be classified into two categories depending on the W/Mo ratio in the starting material: molybdenum-rich educts afford mixtures of microcrystalline hexagonal molybdates together with (W, Mo) oxides (Table 1,

(23) Slade, R. C. T.; Ramanan, A.; Hirst, P. R.; Pressman, H. A. *Mater. Res. Bull.* **1988**, *23*, 793.
(24) Rao, C. N. R.; Deepak, F. L.; Gundiah, G.; Govindaraj, A. *Prog. Solid State Chem.* **2003**, *31*, 5.
(25) Zhou, J.; Deng, S. Z.; Xu, N. S.; Chen, J.; She, J. C. *Appl. Phys. Lett.* **2003**, *83*, 2653.
(26) Zach, M. P.; Inazu, K.; Ng, K. H.; Hemminger, J. C.; Penner, R. M. *Chem. Mater.* **2002**, *14*, 3206.
(27) Lou, X. W.; Zeng, H. C. *J. Am. Chem. Soc.* **2003**, *125*, 2697.
(28) Koltypin, Yu.; Nikitenko, S. I.; Gedanken, A. *J. Mater. Chem.* **2002**, *12*, 1107.
(29) Li, Y. B.; Bando, Y.; Golberg, D.; Kurashima, K. *Chem. Phys. Lett.* **2002**, *367*, 214.
(30) Lee, K.; Seo, W. S.; Park, J. T. *J. Am. Chem. Soc.* **2003**, *125*, 3408.
(31) Zhu, K.; He, H.; Xie, S.; Zhang, X.; Zhou, W.; Jin, S.; Yue, B. *Chem. Phys. Lett.* **2003**, *377*, 317.
(32) Reis, K. P.; Ramanan, A.; Whittingham, M. S. *J. Solid State Chem.* **1991**, *91*, 394.
(33) Zhan, J. H.; Yang, X. G.; Xie, Y.; Li, B. F.; Qain, Y. T.; Jia, Y. B. *Solid State Ionics* **1999**, *126*, 373.
(34) Gier, T. E.; Pease, D. C.; Sleight, A. W.; Bither, T. A. *Inorg. Chem.* **1968**, *7*, 1646.
(35) Dickens, P. G.; Halliwell, A. C.; Murphy, D. J.; Whittingham, M. S. *Trans. Faraday Soc.* **1971**, *67*, 794.
(36) Salje, E.; Gehlig, R.; Viswanathan, K. *J. Solid State Chem.* **1978**, *25*, 239.
(37) Ayyappan, S.; Subbanna, G. N.; Rao, C. N. R. *Chem. Eur. J.* **1995**, *3*, 165.
(38) Michailovski, A.; Krumeich, F.; Patzke, G. R. *J. Solid State. Chem.* submitted for publication.
(39) Michailovski, A.; Krumeich, F.; Patzke, G. R. *Mater. Res. Bull.* submitted for publication.
(40) Cruywagen, J. J.; Heyns, J. B. B. *S. Afr. J. Chem.* **1981**, *34*, 118.
(41) Krebs, B. *Acta Crystallogr.* **1972**, *B28*, 2222.

Table 1. Products Emerging from the Solvothermal Reaction of Yellow Molybdic Acid and Ammonium Metatungstate

exp.	at. % W	at. % Mo	phases	morphology	average diameter	average length
			molybdenum-based series (exp. 1 −5)			
1	0	100	MoO_3	nanorods	200 nm	2−10 μm
2	10	90	hexagonal Mo bronze	hexagonal microcrystals	1−3 μm	> 10 μm
			$W_{1-x}Mo_xO_3 \cdot 0.33H_2O$	hexagonal platelets	120 nm	1−3 μm
			($x = 0.6-0.8$)	few nanorods	200 nm	300−400 nm
3	20	80	hexagonal Mo bronze	hexagonal microcrystals	2 μm	10 μm
			$W_{1-x}Mo_xO_3 \cdot 0.33H_2O$ ($x = 0.7$)	irregular microcrystals		1−2 μm
4	30	70	hexagonal Mo bronze	few microcrystals	2.5 μm	9 μm
			$W_{1-x}Mo_xO_3 \cdot 0.33H_2O$ ($x = 0.6$)	fibrous nanostructures	30 nm	max. 1 μm
5	40	60	hexagonal Mo bronze	few microcrystals	3 μm	15 μm
			$W_{1-x}Mo_xO_3 \cdot 0.33H_2O$			
			$(NH_4)_{0.2}W_{1-x}Mo_xO_3$ ($x = 0.7$)	fibrous nanostructures	40 nm	1 μm
			tungsten-based series (exp. 6 −11)			
6	50	50	hexagonal Mo bronze	decaying microcrystals		few μm
			$(NH_4)_{0.2}W_{1-x}Mo_xO_3$ ($x = 0.7-0.5$)	nanorod structures	30 nm	300−800 nm
7	60	40	$(NH_4)_{0.22}(W_{0.43}Mo_{0.57})O_3$	nanorod structures	30 nm	400 nm − 1 μm
8	70	30	$(NH_4)_{0.22}(W_{0.54}Mo_{0.46})O_3$	nanorod structures	30 nm	1−3 μm
9	80	20	$(NH_4)_{0.20}(W_{0.70}Mo_{0.30})O_3$	nanorod structures	20 nm	200 nm − 1.4 μm
10	90	10	$(NH_4)_{0.27}(W_{0.84}Mo_{0.16})O_3$	nanorod structures	20 nm	1 nm − 2 μm
11	100	0	$(NH_4)_{0.26}WO_3$	nanorods	20 nm	80−200 nm

molybdenum-based series (exp. 1−5) and Figure 1). Increasing tungsten contents (50−100 at. %) give rise to a series of $(NH_4)_x(W,Mo)O_3$ nanorods (Table 1, tungsten-based series (exp. 6−11) and Figure 2). These product classes exhibit the following structural and morphological features.

Tungsten-Based Series. Initial tungsten contents between 50 and 60 at. % trigger the transition from microcrystalline products to phase-pure $(NH_4)_x(W,Mo)O_3$ nanorods. $(NH_4)_{0.22}(W_{0.43}Mo_{0.57})O_3$ nanorods (Table 1, exp. 7) with hexagonal symmetry ($a = 7.29(4)$, $c = 3.88(2)$ Å) are obtained from educts containing 60 at. % tungsten. Their Bragg reflections are fairly broad due to the small particle size (Figure 3). A hexagonal form of WO_3 ($P6/mmm$, $a = 7.298(2)$, $c = 3.899(2)$ Å)[42] was found to be the closest match. Generally, the $(NH_4)_x(W,Mo)O_3$ nanorods exhibit average diameters in the 20−30 nm range and lengths below 1 μm. They assemble into manifold microscale arrangements such as spheres (Figure 2 a), hollow toroids (Figure 2 b), or parallel alignments (Figure 2 c). The entire precursor mixture is transformed quantitatively into a multitude of hierarchical nanorod-based patterns.

Molybdenum-Based Series. The formation of MoO_3 nanorods from yellow molybdic acid (Table 1, exp. 1) ceases when the starting material contains more than 10 at. % tungsten. Hexagonal molybdate microcrystals with diameters of 1−3 μm and lengths around 10 μm (Figure 1 b−d) emerge instead of nanorods. Mixed hexagonal (W, Mo)-microcrystals with irregular crystal shapes are formed as a side product (Figure 1 a and b). Their XRD pattern ($a = 7.312(1)$, $c = 7.683(1)$ Å, cf. exp. 3, Table 1) matches with yet another hexagonal form of WO_3 ($P6_3/mcm$, $a = 7.3244(6)$, $c = 7.6628(5)$ Å).[43] The pure molybdate phase (exp. 3, Table 1) exhibits lattice constants ($a = 10.561(2)$, $c = 3.727(1)$ Å) that are close to the values reported for the hexagonal ammonium molybdenum bronze $(NH_4)_{0.944}H_{3.3}O_4Mo_{5.292}O_{18}$ ($P6_3/m$, $a = 10.5332(1)$, $c = 3.7286(1)$ Å).[44] When the tungsten content is further raised (>30 at. %), the transformation of microcrystals into rod-shaped mixed $(NH_4)_x(W,Mo)O_3$ nanorods nanostructures sets in (Figure 1 c−e).

Characterization of the Mixed Nanorods. The mixed nanorods adopt the net formula $(NH_4)_{0.2}W_{1-x}Mo_xO_3$ ($x = 0.5-0.8$, with x depending on the starting material, cf. Table 1). EDX spot analyses confirmed the simultaneous presence of both molybdenum and tungsten in the individual nanorods (Figure 4). $(NH_4)_{0.21}W_{0.53}Mo_{0.47}O_3$ was selected for further characterizations.

(1) Thermal analysis (Figure 5) revealed a mass loss of 4.9% below 300 °C that is due to adherent traces of water or acetic acid. The subsequent mass loss of 2% is accompanied by a thermal effect at 305 °C and thus corresponds to the total loss of ammonia (theoretical value: 2%). Up to 800 °C, no further mass loss is observed and the thermal effects at 889 °C and 1143 °C do not correspond to the melting points of the binary oxides (MoO_3 and WO_3 melt at 795 °C or 1473 °C, respectively, and the sublimation of MoO_3 starts around 750 °C). The complete evaporation of MoO_3 from the structure would require a mass loss of 44%, which is approximately twice as high as the experimental value of 22% observed in the 800−1200 °C range. The residual material thus represents a hitherto unassigned (Mo,W)-based phase.

(2) After heating to 450 °C, elementary analyses indicate the presence of a *virtually* ammonium-free material, $(NH_4)_{0.01}W_{0.52}Mo_{0.48}O_3$. Figure 6 a and b display representative SEM images of $(NH_4)_{0.21}W_{0.53}Mo_{0.47}O_3$ before heating to 450 °C. The complex morphology withstands the heating process as can be seen from SEM images taken afterward (Figure 6c and d): the nanorod patterns are maintained and the dimensions of the individual nanorods are kept constant. The corresponding XRD patterns (Figure 7 bottom, trace b) indicate the onset of structural transformations around 450 °C. Traces of residual NH_4^+ ions are remaining even after heating to 450 °C, as the characteristic NH_4^+ bending vibrations at 1401 and 1605 cm^{-1} are still present in the IR spectrum of the heated material (Figure 7 top). The small ammonium amounts detected during elementary analysis are obviously essential for stabilizing the hexagonal framework.

(42) Gérand, B.; Nowogrocki, G.; Guenot, J.; Figlarz, M. *J. Solid State Chem.* **1979**, *29*, 429.
(43) Oi, J.; Kishimoto, A.; Kudo, T.; Hiratani, M. *J. Solid State Chem.* **1992**, *96*, 13.
(44) Guo, J. D.; Zavalij, P.; Whittingham, M. S. *J. Solid State Chem.* **1995**, *117*, 323.

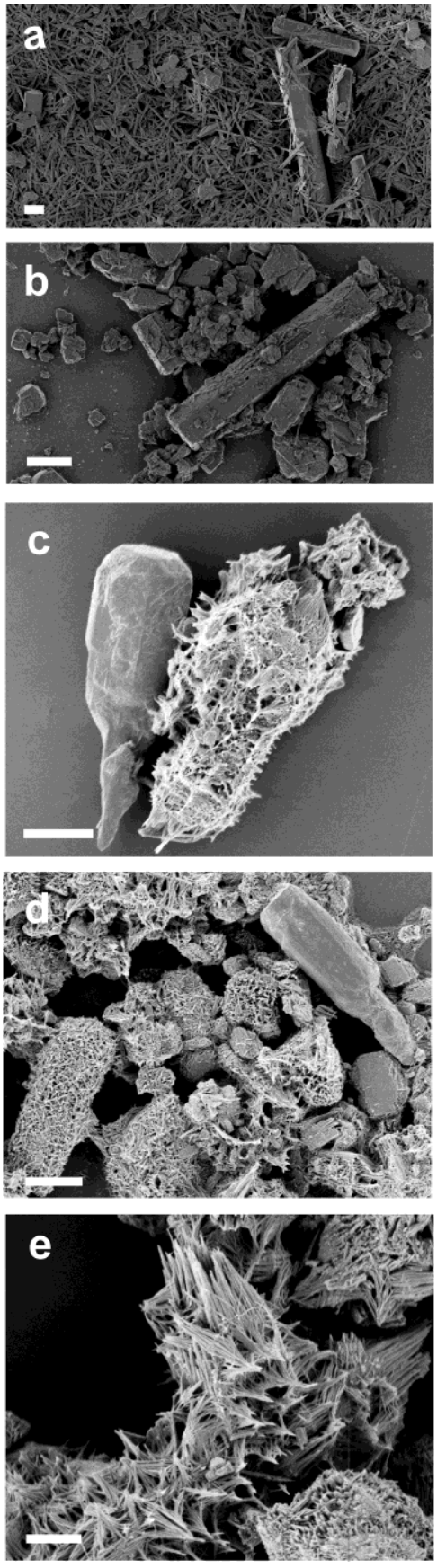

Figure 1. SEM images (scale bar = 2 μm) displaying the effect of increasing tungsten contents in the starting material (cf. molybdenum-based series in Table 1): (a) 10 at. % W (exp. 2); (b) 20 at. % W (exp. 3); (c) 30 at. % W (exp. 4); (d) 35 at. % W; (e) 40 at. % W (exp. 5).

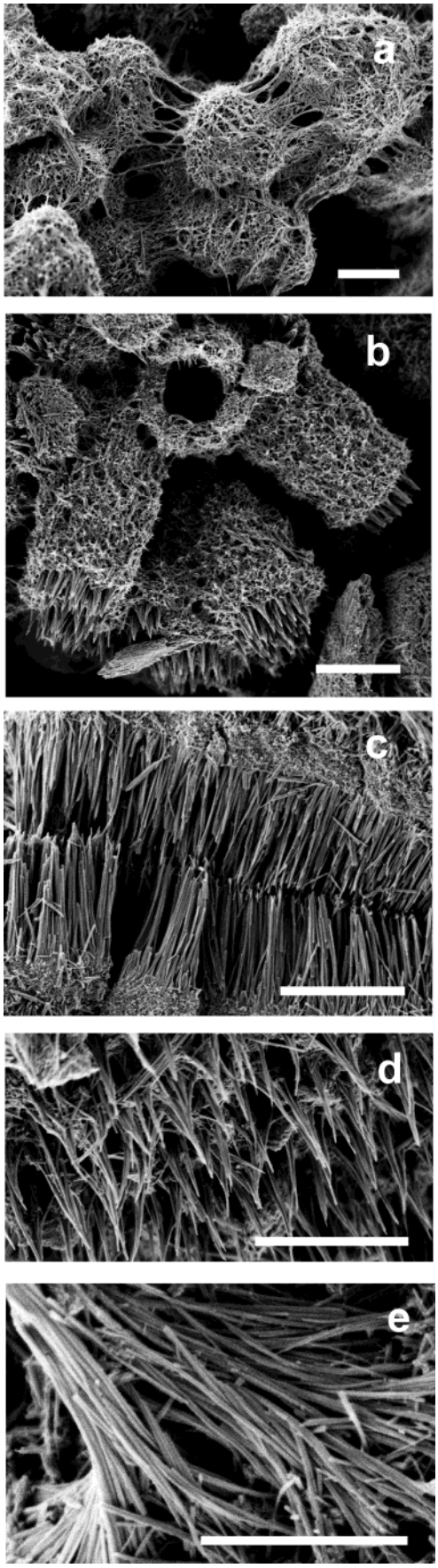

Figure 2. SEM images (scale bar = 2 μm) of mixed $(NH_4)_{0.2}$-$(W,Mo)O_3$ nanorods (cf. tungsten-based series in Table 1): (a) 50 at. % W (exp. 6); (b) 60 at. % W (exp. 7); (c) 70 at. % W (exp. 8); (d) 80 at. % W (exp. 9); (e) 90 at. % W (exp. 10).

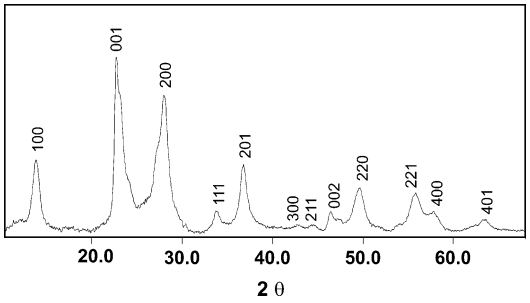

Figure 3. Representative XRD pattern of $(NH_4)_{0.22}(W_{0.43}Mo_{0.57})O_3$ nanorods (cf. Figure 2 b).

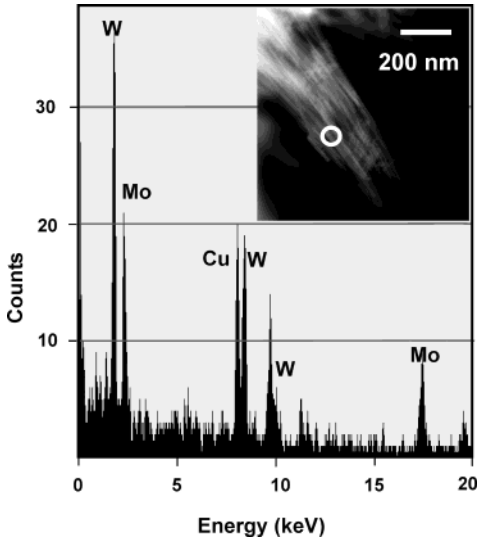

Figure 4. Representative EDX spot analysis conducted on mixed nanorods (cf. exp. 7, Table 1). The STEM image with the beam position marked is shown as inset.

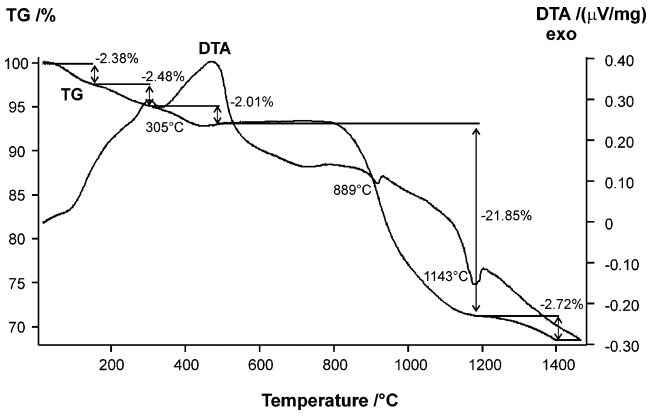

Figure 5. DTA/TG analysis of $(NH_4)_{0.21}W_{0.53}Mo_{0.47}O_3$.

(3) The N_2 Brunauer−Emmett−Teller (BET) surface area of $(NH_4)_{0.21}W_{0.53}Mo_{0.47}O_3$ was found to be 88.9 m^2 g^{-1}. The mixed system therefore exhibits a surface area that exceeds the maximum values for pure MoO_3 nanorods (13 m^2 g^{-1})[8] and for a typical $(NH_4)_{0.26}WO_3$ nanorod sample (37.8 m^2 g^{-1}).[38]

Formation of Mixed Nanorods: Influence of the Reaction Parameters. The solvothermal parameter window required for nanorod formation was investigated. The initial W/Mo ratio was fixed to 0.6:0.4, and the impacts of reaction time and temperature were investigated.

The reaction sets in between 100 and 140 °C. After 4 d of solvothermal treatment at 100 °C, the XRD pattern

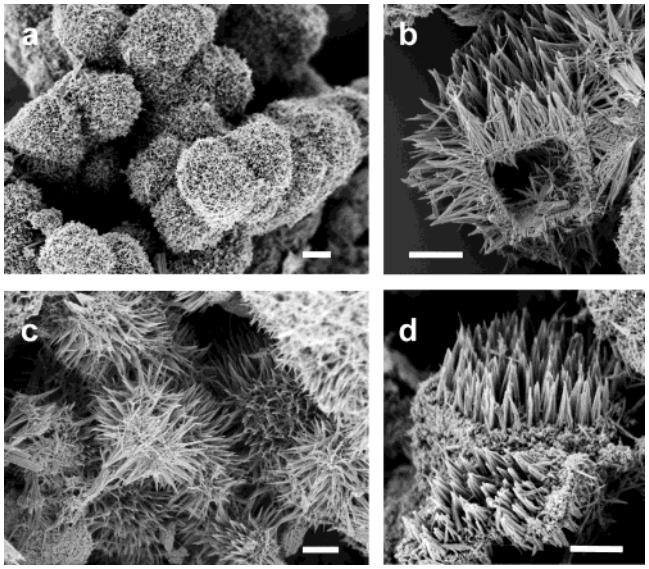

Figure 6. Mixed bronze nanostructures: $(NH_4)_{0.21}W_{0.53}Mo_{0.47}O_3$ before (a, b) and the resulting $(NH_4)_{0.01}W_{0.52}Mo_{0.48}O_3$ after (c, d) heating to 450 °C (SEM images, scale bar = 1 μm).

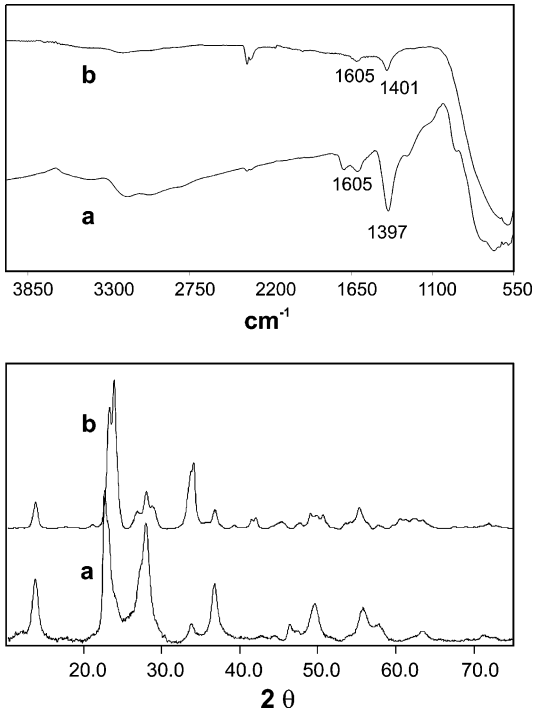

Figure 7. IR spectra (above) and XRD patterns (below) of $(NH_4)_{0.21}W_{0.53}Mo_{0.47}O_3$ before (a) and (b) after heating to 450 °C.

reveals the presence of $(NH_4)_x(W,Mo)O_3$ with only few remaining impurities. Between 100 and 140 °C, microscale agglomerates consisting of very tiny nanorods (Figure 8 a) prevail. The optimum reaction temperature for the self-organization of nanorods into microscale patterns such as hollow tubes (Figure 8 b) is located around 180 °C. A further increase in temperature to 220 °C is counterproductive and gives rise to nanorod agglomeration (bundle-like structures in Figure 8 c).

The typical mixed nanorod growth patterns are already present after 8 h of reaction time (Figure 9 a) and only a few highly agglomerated rod bundles are remaining (Figure 9 b). Their XRD pattern corresponds well to the indexed pattern displayed in Figure 3.

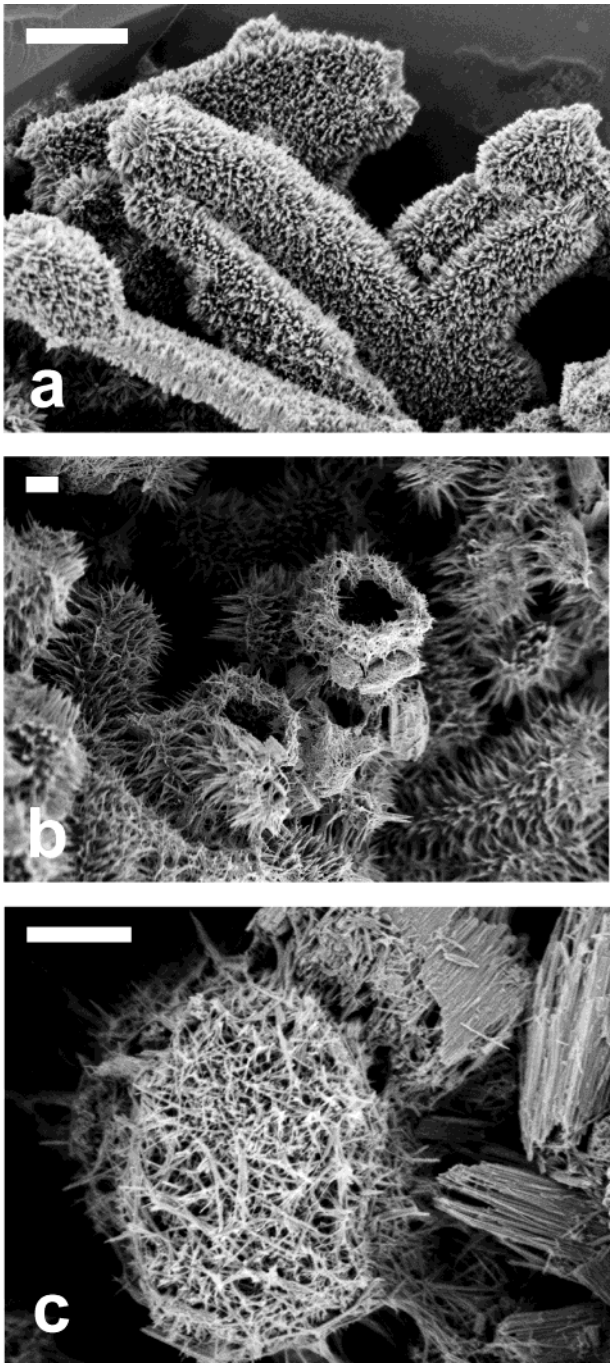

Figure 8. Mixed nanostructures formed after 4 d at (a) 100 °C, (b) 180 °C, and (c) 220 °C (SEM images, scale bar = 1 μm).

Prolonged solvothermal treatments (8 d) still afford the characteristic microscale rod patterns (Figure 9 c), but considerable areas of the sample have collapsed into bundle-like agglomerates again (Figure 9 d). As a consequence, medium reaction times of 2−4 d are most advisable.

Discussion

Characteristics of the Mixed Solvothermal Reaction. There are major morphological differences between the pure molybdenum- and tungsten-based nanorods and their mixed counterparts. The higher the tungsten content in the starting material, the lower the aspect ratio of the emerging nanorods. Figure 10 illustrates this trend. MoO_3 rods (Figure 10 b) display a high degree of anisotropy with diameters in the 100-nm regime and microscale lengths.[8] The mixed rods, however, do not exceed 1 μm in length and exhibit average diameters of 20−30 nm (Figure 10 c). Their aspect ratio thus adopts medium values, because the diameters of pure $(NH_4)_xWO_3$ nanorods are in the same range, whereas their length is further reduced to values below 200 nm (Figure 10 d).[38]

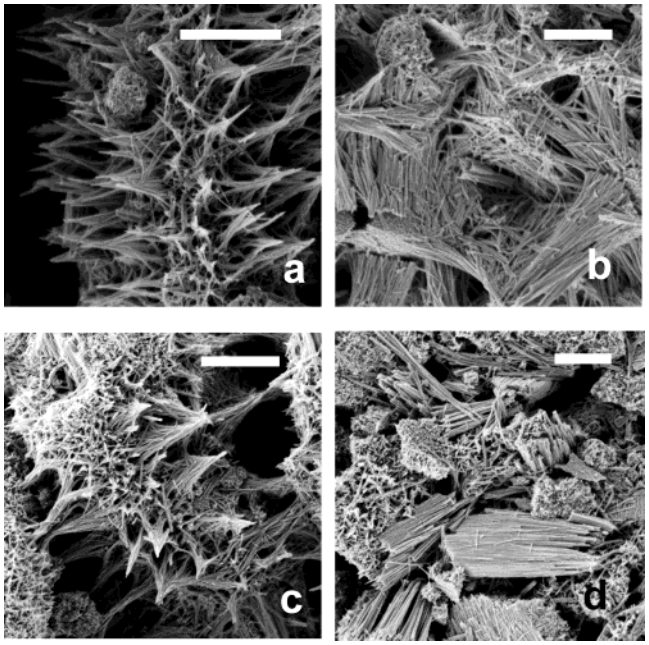

Figure 9. Mixed nanostructured bronzes formed from starting materials with 60 at. % W after 8 h (a, b) and 8 d (c, d) of solvothermal treatment (SEM images, scale bar = 1 μm).

The strong tendency toward self-organization is an exclusive morphological feature of the mixed system and strongly depends on the precursor materials. The combined reaction of layered yellow molybdic acid with its tungsten-based analogue, H_2WO_4, does not give rise to the formation of nanorod patterns. The two-dimensional pre-structuring in layered compounds is predestined to form anisotropic nanoparticles by means of topotactic processes. On the other hand, the numerous nanoscale products that are available from ammonium metatungstate indicate that cluster-containing, nonlayered precursors can be of equal convenience for the solvothermal production of nanoparticles.[38]

The formation process of the nanorod patterns obviously includes the dissolution of microcrystals into nanorods. Intermediate products with hollow interiors in the micrometer range (Figure 11 and Figure 6 a) point to this growth pathway. Moreover, some microcrystals were quenched on their way to nanorods (Figure 12). Figure 1 c shows an unaffected microcrystal side by side with its rod-covered pendant. Thus, the caving of microcrystals by rod growth on their surface might account for the formation of hollow rod arrangements. This assumption is further backed by microcrystals quenched from 100 °C (cf. Figure 8 a): they are covered with a furry layer of tiny rods.

Formation of Ammonium-Free Molybdenum Tungsten Oxides. Whereas the one-step routine presented here is a convenient pathway to mixed bronze systems with a high surface area, the complete removal of ammonium cations from the hexagonal (W, Mo)-oxide

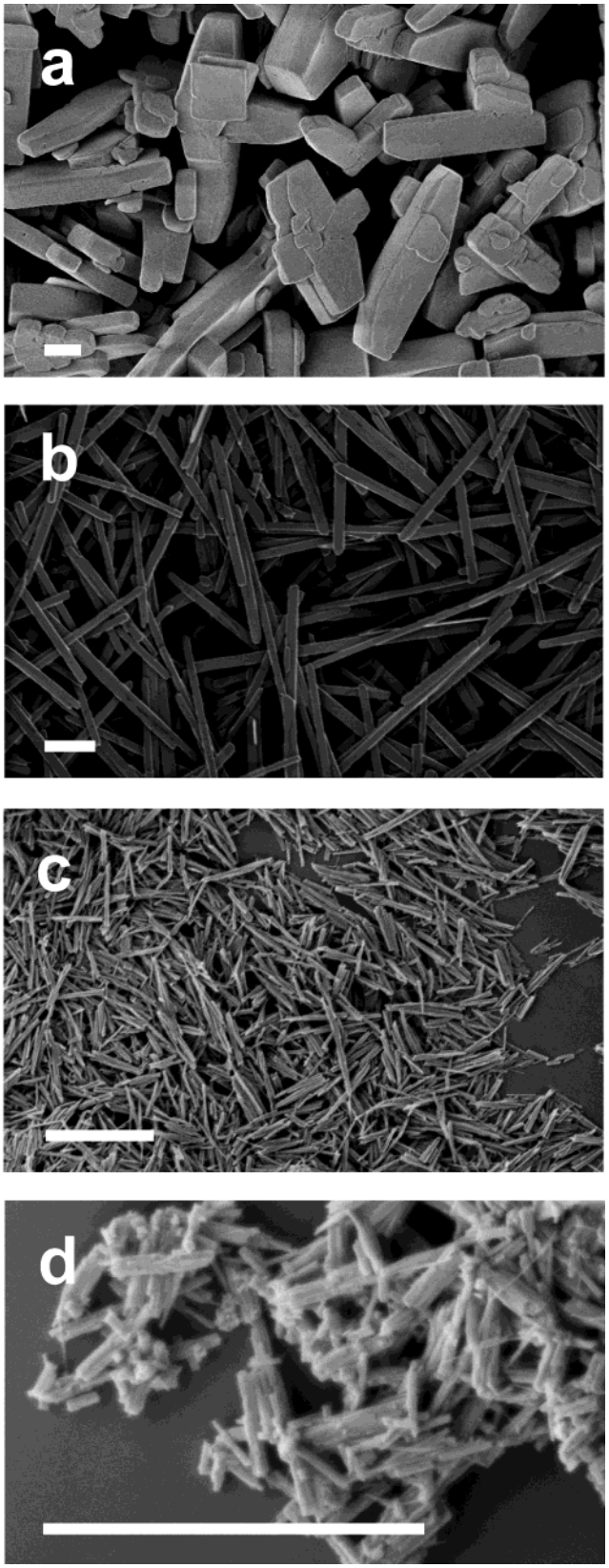

Figure 10. SEM images of (a) the starting material $MoO_3 \cdot 2H_2O$, (b) MoO_3 nanorods, (c) mixed nanorods, and (d) $(NH_4)_{0.26}WO_3$ nanorods (scale bar = 1 μm).

framework remains a preparative challenge. To the best of our knowledge, pure nanoscopic molybdenum tungsten bronzes have never been described. Obviously, the presence of ions in the hexagonal channels is essential for their structural stability. The quest for the pure

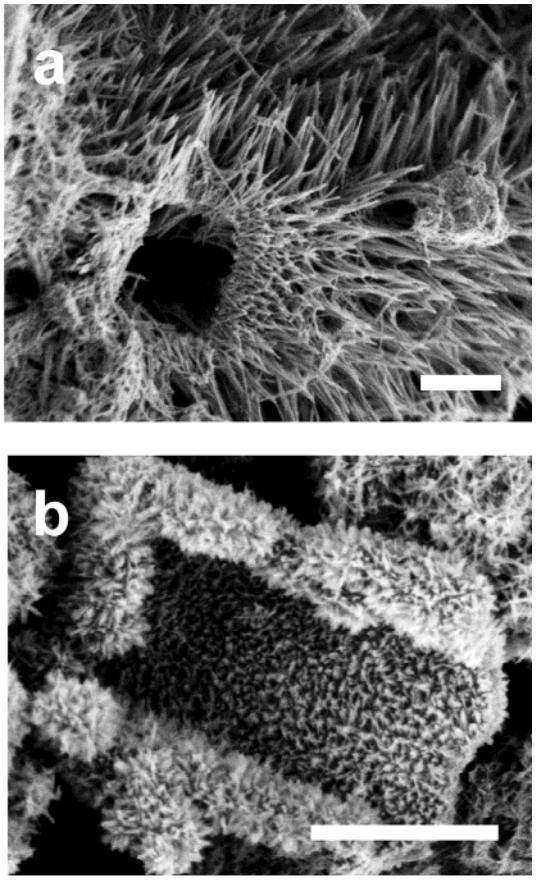

Figure 11. Hollow intermediate structures formed after (a) 2 d at 180 °C and (b) 4 d at 100 °C (SEM images, scale bar = 1 μm).

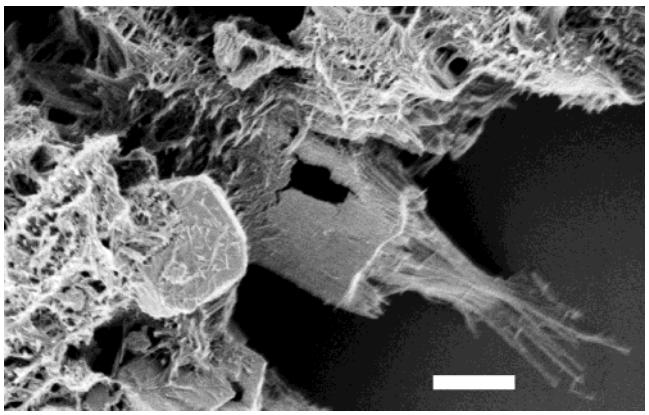

Figure 12. Intermediate structure: microcrystal with emerging nanofibers (SEM image, scale bar = 1 μm).

hexagonal form of MoO_3 documents that considerable experimental effort is necessary to generate an entirely ion-free channel structure, because the stabilizing effect can even be exerted by traces of ions.[44,45] As a consequence, the mixed $(NH_4)(W,Mo)O_3$ nanorods still retain a minimum amount of ammonium ions (that practically falls below the detection limits of elementary analysis) after heating to 450 °C. The presence of highly stabilizing ammonium ions in the solvothermal reaction system might thus account for the exclusive formation of hexagonal phases throughout all experiments performed

(45) Muraoka Y.; Grenier J.-C.; Petit, S.; Pouchard, M. *Solid State Sci.* **1999**, *1*, 133.

in the course of this study.

Conclusion

The combined solvothermal reaction of layered $MoO_3 \cdot 2H_2O$ with the Keggin compound ammonium metatungstate gives rise to mixed $(NH_4)_x(W,Mo)O_3$ bronzes consisting of nanorods with diameters of 20−30 nm and lengths between 200 nm and 1 μm. These nanorods self-organize into a diversity of manifold microscale growth patterns—including spherical and toroidal hollow arrangements—and this phenomenon is reminiscent of biomineralization processes. Surprisingly, these novel nanostructured mixed bronzes maintain their morphological features upon thermal treatment. The combination of precursors with different structural motifs is essential to generate these particles. Further research perspectives are now opening up: first, the growth mechanism leading to the uncommon morphologies remains to be fully enlightened. Second, the properties and possible applications of nanostructured $(NH_4)_x(W,Mo)O_3$ have to be explored. As the nanorods exhibit an unexpected resistance against thermal treatment at 450 °C with their outer shape remaining untouched, there is a good chance that their high BET surface area of 89 $m^2\ g^{-1}$ can be applied at elevated temperatures, e.g., in catalysis.

Acknowledgment. We thank Prof. Dr. R. Nesper (Laboratory of Inorganic Chemistry, ETH Zurich) for his steady interest and the continuous support of this work. Our research was funded by the ETH Zurich, by the Swiss National Science Foundation (MaNEP, Materials with Novel Electronic Properties) and by the National Research Program “Supramolecular Functional Materials”. Special thanks to Dr. Christoph Stinner for the BET measurements and to Christian Mensing for DTA/TG investigations.

CM0311731